An Empirical Model for Correction of Topographic Effect in Microwave Radiation of Mountainous Area

Shaojie Zhao, *Member, IEEE*, Ting Liu, Linna Chai, *Member, IEEE*, Peng Wang, Diyan Chen, and Tao Zhang

***Abstract*—The topographic effect is one of the essential factors affecting microwave radiation in mountainous regions. This effect's correction can improve the inversion accuracy of key surface parameters. Here, a new terrain correction model in microwave pixel scale is proposed by regression. Using the rugosity (RU) measure the relief of land surface, and analyze its correlation with the brightness temperature difference between the undulating surface and flat surface ($\Delta TB_{\varphi Ri}$). The topographic effects are simulated by the mountain microwave radiation model. Through the regression analysis of the topographic effects with RU in different regions, we find that: first, RU has a linear relationship with the average $\Delta TB_{\varphi Ri}$ for different azimuths of the pixel ($\overline{\Delta TB}$), with the value of R^2 above 0.9 for both polarization; then, the effects of azimuths and ground characteristics on brightness temperature can also be corrected by establishing their regression relationship with brightness temperature. Combined with these analyses, an empirical model is developed to measure the topographic effect according to RU. The verification results show that the ΔTB_{model} calculated by the empirical model is similar to the $\Delta TB_{\text{simulated}}$ of microwave radiation model ($r > 0.9$), which indicates that the empirical model is suitable for mountainous areas with different terrains. Results also provide a theoretical basis for improving the accuracy of passive microwave remote sensing of mountainous areas.**

***Index Terms*—Microwave radiation, rugosity (RU), terrain correction model, topographic effect.**

I. Introduction

MOUNTAINS cover about 24% of the Earth's land area and are essential in regulating the regional and global climate environment [1], [2], [3]. However, the topography is one of the critical factors affecting the microwave radiation of pixel-scale in mountainous regions. The complex geometric structure of mountains and the unique water and heat characteristics and ecosystem structure caused by topography can result in the observation error of microwave radiometer [4], [5], [6], [7]. It leads to a lower inversion accuracy of mountain surface soil moisture than flat surface [8], [9], [10]. Research has shown that the error in soil moisture inversion caused by topography can exceed 4% [11].

The microwave radiation of the mountainous region differs from that of a flat surface. The signals received by microwave radiometers mainly include surface radiation and atmospheric radiation. The higher altitude in the mountainous area causes a decrease in atmospheric thickness, which reduces the attenuation of surface microwave radiation and the contribution of atmospheric radiation. The surface radiation is affected by slope, aspect, shading effect, and multiple radiation scattering between mountains. These theories provide the foundation for studying topographic effects [12]. Currently, the topographic effects are considered in many passive microwave remote sensing studies. For example, Kerr et al. [13] integrated DEM into the brightness temperature simulation and evaluated the brightness temperature deviation caused by topographic relief. In the study by Mialon et al. [14] the semi-variogram features of DEM classify topography, and the pixels in which topography has a high impact was marked. A study by Talone et al. [15] analyzed the effects of local incident angle, shadowing, and atmosphere on brightness temperature through model simulations. Pulvirenti et al. [16], [17] developed the Simulator of Topographic Artefacts in MIcrowave RAdiometry (STAMIRA), to predict the topographic relief effects on the measurements of a microwave radiometer. Based on the STAMIRA, they analyzed the impact of elevation, slope, aspect, and local incidence angle on the brightness temperature of microwave radiation. Utku and Vine [18] proposed a probability density function to replace DEM to measure the topographic relief of the surface. The topography is divided into "smooth" and "rough," and the corresponding statistical model is established to predict the topography's impact. Li et al. [11] consider topographic relief as roughness on the pixel scale and uses the standard deviation in elevation and correlation length descrifacetg the rough surface to quantify the complexity of the topography.

These studies usually correct the terrain effect according to the relationship between the geometric characteristics of the terrain and the brightness temperature [13], [14], [15], [16], [18], [19], [20], [21], [22], [23], [24]. However, there are few

Manuscript received 31 March 2023; revised 1 July 2023 and 2 September 2023; accepted 13 September 2023. Date of publication 28 September 2023; date of current version 16 October 2023. This work was supported in part by the National Natural Science Foundation of China under Grant 41871228 and Grant 42171319 and in part by the Second Tibetan Plateau Scientific Expedition and Research Program (STEP) under Grant 2019QZKK0306. *(Corresponding author: Ting Liu.)*

Shaojie Zhao, Linna Chai, and Diyan Chen are with the State Key Laboratory of Earth Surface Processes and Resource Ecology, Faculty of Geographical Science, Beijing Normal University, Beijing 100875, China (e-mail: shaojie.zhao@bnu.edu.cn; chai@bnu.edu.cn; 202121051068@mail.bnu.edu.cn).

Ting Liu is with the State Key Laboratory of Earth Surface Processes and Resource Ecology, Faculty of Geographical Science, Beijing Normal University, Beijing 100875, China, and also with the Land Satellite Remote Sensing Application Center, MNR, Beijing 100048, China (e-mail: 201921120046@mail.bnu.edu.cn).

Peng Wang is with the College of Geoexploration Science and Technology, Jilin University, Changchun 130012, China (e-mail: wpeng21@mails.jlu.edu.cn).

Tao Zhang is with the Land Satellite Remote Sensing Application Center, MNR, Beijing 100048, China (e-mail: zhangtao@mail.bnu.edu.cn).

Digital Object Identifier 10.1109/JSTARS.2023.3320548

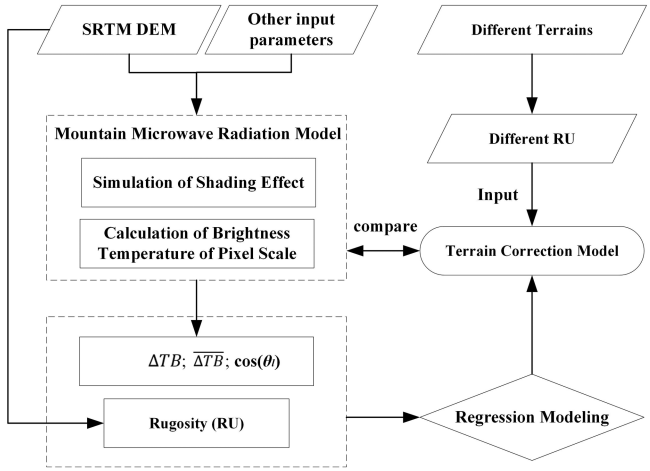

Fig. 1. Flowchart of the terrain effect simulation and regression modeling.

studies on measuring the relief of land surface and the influence of that on surface microwave radiation. Li et al. [11] used the roughness to quantify the relief of land surface, but it does not obtain the relationship between topographic effects and the relief of land surface. In addition, the methods of simulating microwave radiation brightness temperature are different in different studies. Most studies did not consider the impact of azimuth observation angle. Although Flores et al. [6] considered the effect of azimuth observation angle, the simulation was based on simulated terrain, which is quite different from terrains in the real world. Therefore, it is necessary to study further the influence of observation azimuth and the relief of the land surface on microwave radiation.

In this article, we propose a new statistical model to predict the impact of topography on microwave radiation. For this purpose, DEM is used to calculate the relief of the land surface in pixel scale surface. The microwave radiation model simulates the topographic effects of different terrain areas, which include local incidence angle, polarization rotation angle, observation orientation, and shading effect. Moreover, accounting for the influence of ground characteristics on microwave radiation, the impact of soil moisture and temperature on brightness temperature is also analyzed. The technology road mapping of this paper is shown in Fig. 1.

The rest of this article is organized as follows. Section II presents the improved microwave radiation model. Section III includes the simulation of topographic effects and the analysis of the influence of topography on brightness temperature. In Section IV, a new model is established by regression analysis to correct the influence of terrain according to the empirical relationship between terrain characteristics and brightness temperature. Finally, Section VI concludes the article.

II. Methods

A. Microwave Radiation Model of Mountain Areas

1) Microwave Radiation of Oblique Surface: The surface brightness temperature observed by the microwave radiometer is proportional to the surface physical temperature (T_{lst}) and the surface emissivity [25]. The brightness temperature (T_{Bp}) can be expressed as

$$T_{Bp} = (1 - \Gamma_p(\theta)) \cdot T_{\text{lst}} \tag{1}$$

where θ is the observation angle of the radiometer, $\Gamma_p(\theta)$ represents the reflectivity of the surface facet, and p represents the polarization mode.

The oblique surface changes the local observation angle. The local observation angle of the surface facet is the angle between the radiometer's observation direction and the surface facet's normal vector, which is expressed by the cosine of the local incident angle ($\cos\theta_l$) [12]

$$\cos\theta_l = \sin\theta_R \ \sin\theta_e \cos\varphi_e + \cos\theta_R \cos\theta_e. \tag{2}$$

In (2), θ_R is the global incidence angle of the radiometer in the observation direction, θ_e is the slope angle of the surface facet, and φ_e is the azimuth angle of the surface facet relative to the observation direction, which is the due north direction (azimuth angle 0° of the global coordinate system). If the azimuth angle of the observation φ_R is not 0°, the local incident angle is expressed as

$$\cos\theta_l = \sin\theta_R \ \sin\theta_e \cos(\varphi_R - \varphi_e) + \cos\theta_R \cos\theta_e. \tag{3}$$

Due to the change of the slope surface facet relative to the horizontal plane, the principal plane of the radiometer observation is changed. Define χ as the polarization rotation angle, then

$$\sin\chi = \frac{\sin\varphi_e \sin\theta_e}{\sin\theta_l}. \tag{4}$$

Similar to (3), if the azimuth angle of the observation φ_R is not 0°, $\sin\chi$ is expressed as

$$\sin\chi = \frac{|\sin(\varphi_R - \varphi_e)| \sin\theta_e}{\sin\theta_l}. \tag{5}$$

According to the local incident angle, the Fresnel formula can be used to calculate the reflectivity of the surface facet in the observation direction of the radiometer in the local coordinate system

$$\Gamma_h\ (\theta_l) = \left| \frac{\cos\theta_l - \sqrt{\varepsilon - \sin^2\theta_l}}{\cos\theta_l + \sqrt{\varepsilon - \sin^2\theta_l}} \right|^2 \tag{6}$$

$$\Gamma_v\ (\theta_l) = \left| \frac{\varepsilon\cos\theta_l - \sqrt{\varepsilon - \sin^2\theta_l}}{\varepsilon\cos\theta_l + \sqrt{\varepsilon - \sin^2\theta_l}} \right|^2 \tag{7}$$

where $\Gamma_h(\theta_l)$ is the reflectivity of horizontal polarization, $\Gamma_v(\theta_l)$ is the reflectivity of vertical polarization, ε is the soil dielectric constant, calculated by the soil dielectric constant model [26]. Then, the reflectivity of the oblique surface can be determined by [12]

$$\Gamma_h\ (\theta) = \Gamma_v\ (\theta_l) \sin^2\chi + \Gamma_h\ (\theta_l) \cos^2\chi \tag{8}$$

$$\Gamma_v\ (\theta) = \Gamma_v\ (\theta_l) \cos^2\chi + \Gamma_h\ (\theta_l) \sin^2\chi. \tag{9}$$

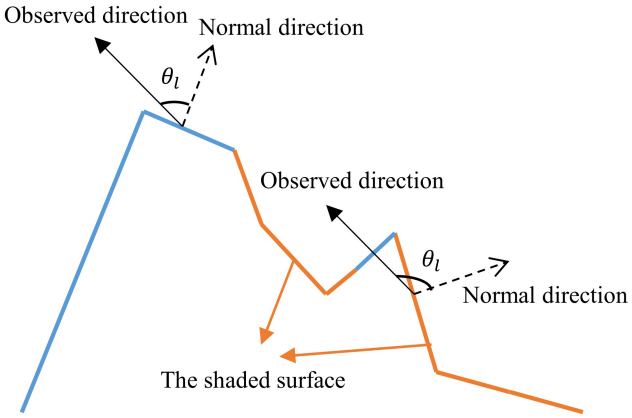

Fig. 2. Schematic illustration of the shading effect. The orange-red area is the shaded surface, which cannot be observed by microwave radiometer.

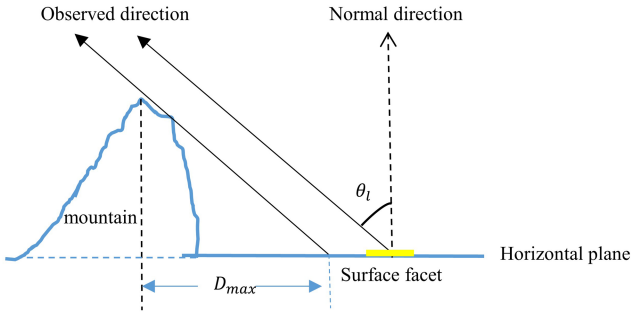

Fig. 3. Shading effect of surrounding mountains.

2) Shading Effect: We assume that the wavelength is much smaller than the scales of the topography. Then we can assume geometrical optics to determine visible and shadowed surface elements. In the pixel scale, some surface facets cannot be observed by the radiometer because they are back in the observation direction of the radiometer or are shaded by the surrounding tall mountains. These surface facets should be excluded from calculating the pixel brightness temperature. Once the observation direction is determined, we can first determine whether the facets in the pixel can be observed by the radiometer according to their slope and aspect and then further screen out the elements that are blocked by the high mountains.

It can be seen fromFig. 2 that when $\theta_l < 90°$, the facets can be observed; when $\theta_l \geq 90°$, that is $\cos\theta_l \leq 0$, the facet cannot be observed. Through the local incident angle, it can be preliminarily judged whether the surface element can be observed according to the slope aspect of the surface element itself.

However, some surface facets with $\theta_l < 90°$ may be shaded by the surrounding mountains in the observation direction. Firstly, the maximum elevation difference H_Δ of the facets in the study area is calculated, and the maximum possible shielding distance($D_{\max}$)is calculated according to the maximum elevation difference (see Fig. 3)

$$D_{\max} = H_\Delta \cdot \tan\theta_R \ . \tag{10}$$

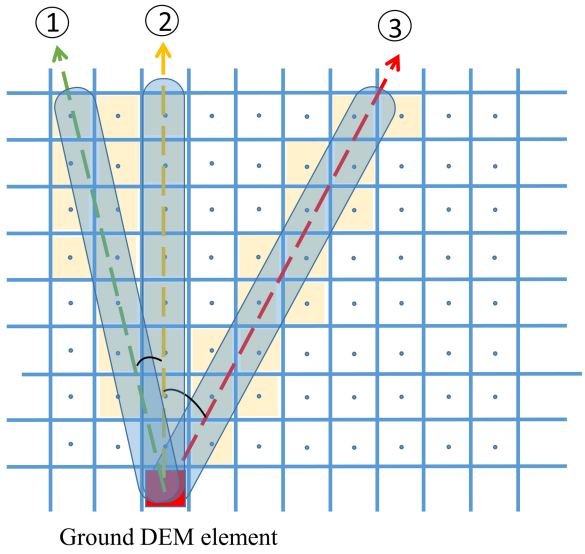

Fig. 4. Facet distribution involved in occlusion calculation. The serial number represents three different observation directions.

In the process of judging whether the facet in the pixel is occluded one by one, it is necessary to calculate whether the terrain blocks the element within the distance $D_{\max}$ in the observation direction and the terrain elements beyond the $D_{\max}$ is not required to participate in the calculation.

If the azimuth angle of the observation is parallel to the row or column direction (corresponding to case ② in Fig. 4), it's straightforward to estimate whether the terrain facet (the red facet in Fig. 4) is shaded by the terrain facets along the column direction one by one. However, for other observing directions, the terrain facet might be shaded by terrain constituted by two adjacent facets (two yellow facets in the same row in Fig. 4). In these situations, the height of the terrain constituted by two adjacent facets is calculated by the weighted sum of the height of the two adjacent facets. The weights of each constituent facet are inversely proportional to the distance between the center of the constituent facets and the line of the observing direction.

3) Brightness Temperature of Pixel Scale: The energy observed by microwave radiometer is the sum of the energy contributed by all facets in the antenna's field of view. we assume that the directivity of each direction in the half power beam width of the antenna is the same, and the energy contributed by all the facets in the antenna field of view is the same [16]. So, the surface brightness temperature observed by the radiometer can be expressed as follows:

$$T_A = \frac{\sum_{i=1}^{N} T_{Bi}\Omega_i}{\sum_{i=1}^{N} \Omega_i} \tag{11}$$

where Ω_i is the solid angle of each patch on the antenna, which can be expressed as follows:

$$\Omega_i = \frac{A\cos\theta_{li}}{R^2\cos\theta_{ei}} \ . \tag{12}$$

Combining the above two formulas, the pixel brightness temperature can be expressed as follows:

$$T_A = \frac{\sum_{i=1}^{N} T_{Bi} \frac{\cos\theta_{li}}{\cos\theta_{ei}}}{\sum_{i=1}^{N} \frac{\cos\theta_{li}}{\cos\theta_{ei}}} \tag{13}$$

where the θ_{li} and θ_{ei} are the local incident angle and slope of the ith DEM element, R is the distance from the radiometer to the ground, A is the projection area at the level corresponding to each bin, and T_{Bi} is the microwave radiation brightness temperature of the ith element.

B. Regression Modeling

This article used a terrain relief factor (R_f) of surface pixels to measure the complexity of terrain. Considering the effects of local incidence angle, polarization rotation, observation azimuth, surface temperature, and soil moisture on brightness temperature, we used the least squares method to establish a regression model between brightness temperature and terrain relief factor. The different azimuth angles of pixels are affected by polarization rotation and terrain occlusion, resulting in significant differences in simulated brightness temperature. Therefore, using brightness temperature at a certain azimuth angle cannot reflect the brightness temperature difference caused by the overall terrain of the pixel. So, in the modeling process, we chose the average brightness temperature ($\overline{\Delta TB}_{\text{model}}$) of each azimuth of the pixel as the breakthrough point. Our purpose was to weaken the influence of azimuth on brightness temperature. Then, as for the brightness temperature at each azimuth (ΔTB_{model}), we calculated it by using the average value with the local incidence angle at each azimuth

$$\overline{\Delta TB}_{\text{model}}\ (\theta_R, p) = \alpha_{\text{slope}}\ (\theta_R, p)\, R_f + \alpha_{\text{intercept}}\ (\theta_R, p) \tag{14}$$

$$\Delta TB\ (\theta_R, \varphi_{Ri}, p) = TB_{\text{mountain}}\ (\theta_R, \varphi_{Ri}, p) - TB_{\text{flat}}\ (\theta_R, p) \tag{15}$$

$$\overline{\Delta TB}\ (\theta_R, p) = \frac{\sum_{i=0}^{n} \Delta TB\ (\theta_R, \varphi_{Ri}, p)}{n} \tag{16}$$

where p is the polarization mode, the global incidence angle θ_R is set to 55°; TB_{mountain} is the simulated brightness temperature of the relief surface, TB_{flat} is the simulated brightness temperature of the flat surface; R_f is topographic factor, α_{slope}, $\alpha_{\text{intercept}}$ are the slope and intercept of the fitting line, respectively; $\overline{\Delta TB}$ is the average $\Delta TB(\varphi_{Ri})$ of the pixel ($i = 0°$,10°,20°, …, 350°)

$$\Delta TB_{\text{model}}\ (\varphi_{Ri}, \theta_R, p) = \left(\cos\theta_i - \overline{\cos\theta}\right)\ \beta_{\text{slope}}\ (\theta_R, p) + \overline{\Delta TB}_{\text{model}}\ (\theta_R, p) \tag{17}$$

where φ_{Ri} is the azimuth angle, $\cos\theta_i$ is value of cos(θ) of the pixel when the azimuth angle is φ_{Ri}, $\overline{\cos\theta}$ is the average of $\cos\theta_i$, β_{slope} is the slope of the fitting line of ΔTB and cos(θ).

The coefficient of determination ($\underline{R}^2$) and root mean square error (RMSE) are important statistical indicators of evaluating the accuracy of regression model. The R^2 and RMSE can be expressed as follows:

$$R^2 = 1 - \frac{\sum_{i=0}^{n} \left(\Delta TB_{\text{simulated}}\ (i) - \Delta TB_{\text{model}}\ (i)\right)^2}{\sum_{i=0}^{n} \left(\Delta TB_{\text{simulated}}\ (i) - \overline{\Delta TB}_{\text{simulated}}\ (i)\right)^2} \tag{18}$$

$$\text{RMSE} = \sqrt{\frac{1}{n} \sum_{i=1}^{n} \left(\Delta TB_{\text{simulated}}\ (i) - \Delta TB_{\text{model}}\ (i)\right)^2} \tag{19}$$

where $\Delta TB_{\text{simulated}}$ refers to the brightness temperature calculated by the microwave radiation model, ΔTB_{model} is the brightness temperature of regression model, $\overline{\Delta TB}_{\text{simulated}}$ is the mean of $\Delta TB_{\text{simulated}}$.

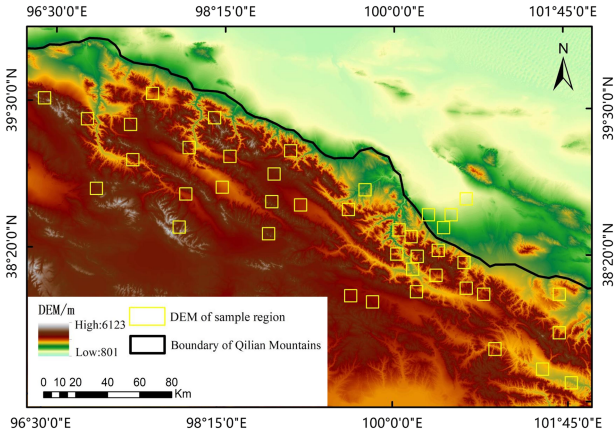

Fig. 5. Distribution of the DEM for 41 sample pixels (10 km × 10 km) of different topographic regions in the northern region of the Qilian Mountains. The regions in the yellow box are the sample regions.

III. Evaluation of Topographic Effects at the Pixel Scale

Before building the terrain correction model, we need to analyze the impact of terrain and features on brightness temperature first. This will help us to determine which terrain factors are involved in the modeling work. This section is mainly divided into four parts, the details are as follows: In Section III-A, we analyzed the variation of brightness temperature with the size of topographic relief. In Section III-B, we selected terrain relief factors to measure the size of the terrain. In Section III-C, we analyzed the influence of soil moisture and temperature on brightness temperature. In Section IV-D, we analyzed the influence of azimuth on brightness temperature. Then, we established a terrain correction model based on the analysis results (see Section IV).

The DEMs used for the microwave radiation model are distributed in the northern region of the Qilian Mountains with complex topography. Considering the complexity of the terrain, we select pixels in different parts of the mountain (peaks, ridges, valleys, saddles, and cliffs). The topographic relief of the sample pixels basically covers all the ranges that can be achieved and is evenly distributed. 41 10 km × 10 km regions were selected to evaluate the topographic effects in pixel scale. These regions are shown in Fig. 5 by the boxes with yellow boundaries. The DEM

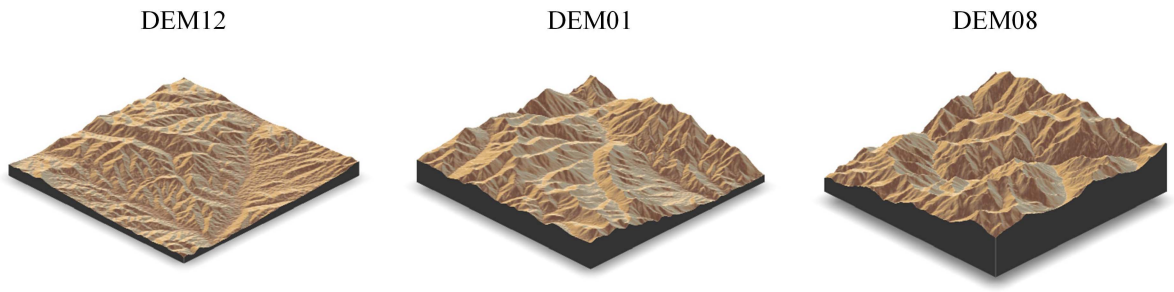

Fig. 6. Shaded-relief maps of three sample pixels with different relief.

TABLE I
TOPOGRAPHIC FACTORS (RA, CEV, AND RU) OF 41 SAMPLE PIXELS

Sample pixels	RA(m)	CEV	RU	Sample pixels	RA(m)	CEV	RU
DEM01	1324	0.079436	1.100583	DEM22	2227	0.131147	1.191759
DEM02	1085	0.056444	1.094151	DEM23	2442	0.128531	1.238568
DEM03	1825	0.095503	1.196829	DEM24	1982	0.109408	1.161854
DEM04	2170	0.115224	1.208976	DEM25	1104	0.051908	1.093260
DEM05	1302	0.072741	1.077245	DEM26	191	0.010171	1.004609
DEM06	1778	0.127765	1.165478	DEM27	495	0.030614	1.002715
DEM07	1050	0.047315	1.090740	DEM28	589	0.028692	1.010611
DEM08	2446	0.131245	1.244118	DEM29	1674	0.076739	1.104063
DEM09	1038	0.076417	1.006626	DEM30	2286	0.131846	1.219359
DEM10	1157	0.071337	1.086326	DEM31	1269	0.080546	1.083948
DEM11	309	0.043850	1.001101	DEM32	1019	0.040238	1.065114
DEM12	664	0.049016	1.030533	DEM33	811	0.039293	1.025271
DEM13	156	0.021337	1.000604	DEM34	2379	0.123913	1.241232
DEM14	1590	0.105250	1.117930	DEM35	1476	0.081711	1.086142
DEM15	842	0.043014	1.037025	DEM36	955	0.042100	1.055197
DEM16	320	0.023467	1.003357	DEM37	2213	0.102029	1.212573
DEM17	1268	0.073494	1.115464	DEM38	1725	0.069024	1.158961
DEM18	193	0.008710	1.001438	DEM39	1627	0.080652	1.197113
DEM19	312	0.013889	1.001919	DEM40	1456	0.067545	1.137834
DEM20	870	0.071053	1.085610	DEM41	1739	0.102203	1.194915
DEM21	496	0.040878	1.004274				

data are obtained from the Shuttle Radar Topography Mission (SRTM) with a spatial resolution of 30 m. Fig. 6 shows the topography of three sample pixels with different topographic regions. It can be seen that there are significant differences in the terrain of different pixel areas.

There are mainly several common terrain relief factor (R_f) of surface pixels, such as rugosity (RU) [27], relief amplitude (RA) [28], and coefficient of elevation variation (CEV)[29]. RA is the difference between the highest and lowest elevations within the DEM. CEV is the ratio of elevation standard deviation to mean elevation within the DEM. RU defined as the ratio of the surface area of the sample pixel to its projection area. The values of RA, RU, and CEV of 41 sample pixels are given in Table I

$$\mathrm{RA} = H_{\max} - H_{\min} \tag{20}$$

$$\mathrm{CEV} = \frac{\sqrt{\frac{1}{n}\sum_{i=1}^{n}\left(H_i - \bar{H}\right)^2}}{\bar{H}} \tag{21}$$

$$\mathrm{RU} = \frac{\mathrm{S_{3D}}}{\mathrm{S_{2D}}}. \tag{22}$$

In (20), $H_{\max}$ and $H_{\min}$ are the maximum and minimum altitudes of the elements within the sample pixel, respectively.

In (21), n is the number of elements within the sample pixel, H_i is the altitude of the ith elements, $\bar{H}$ is the average altitude of the sample pixel.

In (22), $\mathrm{S_{3D}}$ is the surface area of the sample pixel, $\mathrm{S_{2D}}$ is the projection area of sample pixel. In this article, S are calculated using the surface volume (3-D Analyst) toolset of ArcGIS.

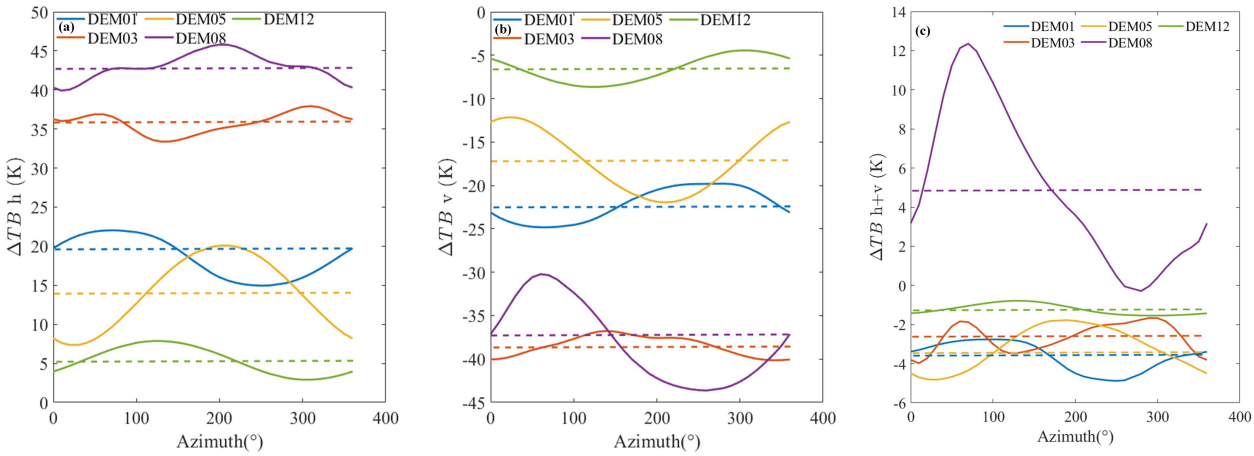

Fig. 7. Simulated ΔTB for different topography regions and azimuth angles. Different colors represent different terrain. The dashed line indicates the $\overline{\Delta TB}$ of each azimuthal angle of the sample pixel.

A. Simulations and Analysis of Mountainous Microwave Radiation

In this word, $\Delta \boldsymbol{TB}_{\varphi_{Ri}}$ is used to represent the effect of topography. In (15), values of TB_{mountain} and TB_{flat} are calculated by the microwave radiation model. The input parameters of the model are as follows: soil moisture that is equal to 0.25 cm^3/cm^3, the surface temperature that is equal to 25 °C, soil bulk density that is equal to 1.3 g/cm^3, and fractions of sand and clay that are equal to 40% and 20%, respectively. The Dobson model calculates the soil dielectric constant for the simulation [26]. For brightness temperature simulations on flat surfaces, Fresnel's reflectivity equation's [30] is used to calculate the surface emissivity and then the brightness temperature, this is because the altitude of different face elements within the pixel is equal, and the local incident angle and rotational polarization will not change due to the observation azimuth. Unlike the flat surface, the microwave radiation of the undulating surface is affected by topographic effects such as local incident angle, polarization rotation angle, and terrain occlusion, and the brightness temperature is different in various observation directions.

The above simulation is based on a homogeneous surface, which assumes that the ground features such as soil moisture, soil texture, and temperature are equal in all elements within the pixel. In the microwave radiation model, the influence of surface roughness and vegetation is not considered to reduce the amount of calculation. Only the ΔTB at the observation angle of 55 ° is simulated. So, the ΔTB of the real surface is lower than this article simulated value.

Fig. 7 shows the ΔTB of six undulating surfaces selected from 41 sample pixels. The solid line in the figure shows the variation of ΔTB with azimuth, and the dashed line indicates the average brightness temperature difference ($\overline{\Delta TB}$) for each azimuth of the same sample pixel. Fig. 7(a) and (b) shows that the trends of ΔTB changing with azimuth are varied for different terrains, and the fluctuation ranges of ΔTB for different observation azimuths are also different. For different terrains, the $\overline{\Delta TB}$ varies from a few K to tens of K, and the $\overline{\Delta TB}$ is related to the relief of land surface within the sample pixel.

In Fig. 7(c), we analyzed the influence of topography on the sum of horizontal polarization and vertical polarization. The results show that, compared with horizontal polarization or vertical polarization, the summation of horizontal and vertical polarization is less affected by land surface relief. This also leads to a smaller difference impact of different terrain relief on the brightness temperature. The analysis of the terrain effect still needs to analyze horizontal polarization and vertical polarization separately.

B. Correlation Between the $\overline{\Delta TB}$ and RU, RA and CEV

To clarify the relationship between the $\overline{\Delta TB}$ and terrain relief, the $\overline{\Delta TB}$ of 41 sample regions is calculated by the method in Section II-A. The relationship between the $\overline{\Delta TB}$ and RU, RA, and CEV is shown in Fig. 8. When RA, CEV is equal to 0 and RU is equal to 1, the surface is flat and the $\overline{\Delta TB}$ is 0 K, with the increase of RU, RA, and CEV, the value of $\overline{\Delta TB}$ increases, and the maximum value is higher than 40K. The figure shows that the relationship between $\overline{\Delta TB}$ and RU, RA, and CEV is linear, and the best linear relationship between $\overline{\Delta TB}$ and RU, with an R^2 value reaching 0.99 ($p<0.01$). Therefore, using RU to measure the relief of land surface, the relationship between the relief of land surface and the $\overline{\Delta TB}$ can be accurately measured of the sample pixel.

C. Effect of Soil Moisture and Temperature on $\overline{\Delta TB}$

To investigate the effect of soil moisture and soil temperature on $\overline{\Delta TB}$ in different topography regions, the $\overline{\Delta TB}$ is simulated at different temperatures (5 °C –40 °C with 1 °C interval) and soil moisture (0.01–0.50 cm^3/cm^3 with 0.01 cm^3/cm^3 interval) while changing only the temperature or soil moisture. The variation trend of $\overline{\Delta TB}$ with soil moisture is shown in Fig. 9, it can be seen that the trends of $\overline{\Delta TB}$ with soil moisture is different for varies of topography regions. Comparing trends in different terrains, it

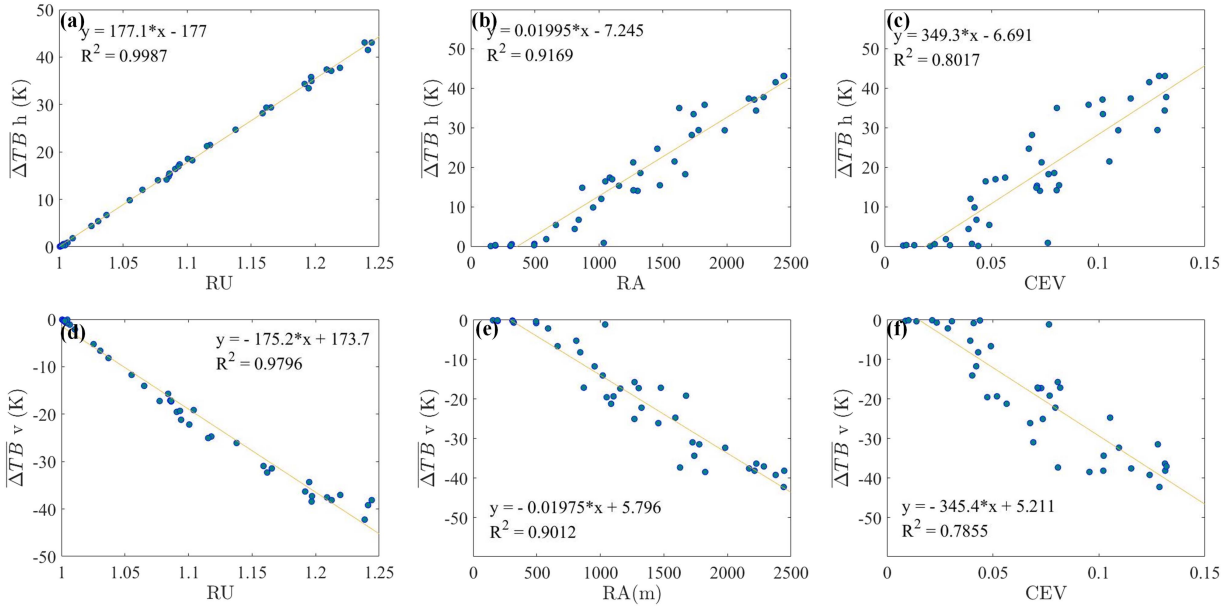

Fig. 8. Correlation between the relief of land surface (RU, RA, and CEV) and $\overline{\Delta TB}$ of 41 sample pixels. The $\overline{\Delta TB}$ is the simulation result of microwave radiation when soil moisture is set to 0.25 and temperature is set to 25 °C.

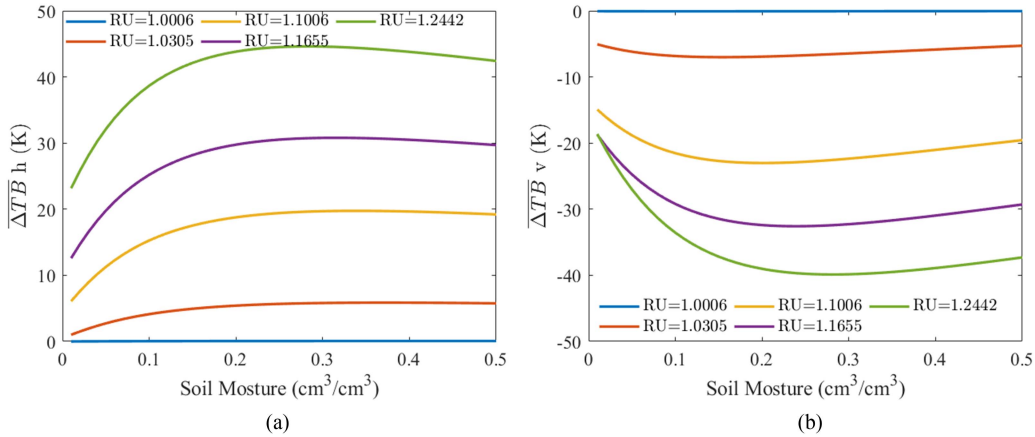

Fig. 9. Variations of $\overline{\Delta TB}$ with soil moisture in different topography regions. Different color represents different relief, the $\overline{\Delta TB}$ is the simulation result of microwave radiation when temperature is set to 25C.

is found that the greater the RU, the greater the influence of soil moisture on $\overline{\Delta TB}$. Different soil moisture makes the value of $\overline{\Delta TB}$ change 0–21K. for soil moisture of 0.01–0.25 cm^3/cm^3, $\overline{\Delta TB}$ increases with increasing soil moisture; for 0.25–0.50 cm^3/cm^3, $\overline{\Delta TB}$ goes down with increasing soil moisture content, and for soil moisture below 0.10 cm^3/cm^3, the effect of soil moisture change on $\overline{\Delta TB}$ was maximum. Fig. 10 shows the tendency of $\overline{\Delta TB}$ with temperature. As with soil moisture, the greater the RU, the greater the effect of temperature on $\overline{\Delta TB}$. The value of $\overline{\Delta TB}$ increases with increasing temperature, for different topography regions, the influence of temperature (from 5 °C to 40 °C) on $\overline{\Delta TB}$ does not exceed 5 K. For most undulating surfaces, the effect of temperature on $\overline{\Delta TB}$ does not exceed 2K.

Compared with temperature, the influence of soil moisture on $\overline{\Delta TB}$ cannot be ignored. The effect of soil moisture should also be considered in the subsequent brightness temperature correction. The terrain correction model established in this way may make soil moisture's inversion result closer to the real surface's value.

D. *Effect of Observation Azimuth on* ΔTB

In terrain surface, the pixel's shading effect, local incident angle, and polarization rotation angle will change with observation orientations. The radiometer will receive the radiation emitted from the surface of different regions in the pixel at different azimuth angles. Fig. 11 shows the shading effect of DEM08, the largest RU of 41 sample pixels, at a global observation angle of 55° of the radiometer, for different observation azimuths. In Fig. 11, the north direction is 0° observation orientation, black area is blocked area. The ΔTB output by the mountain

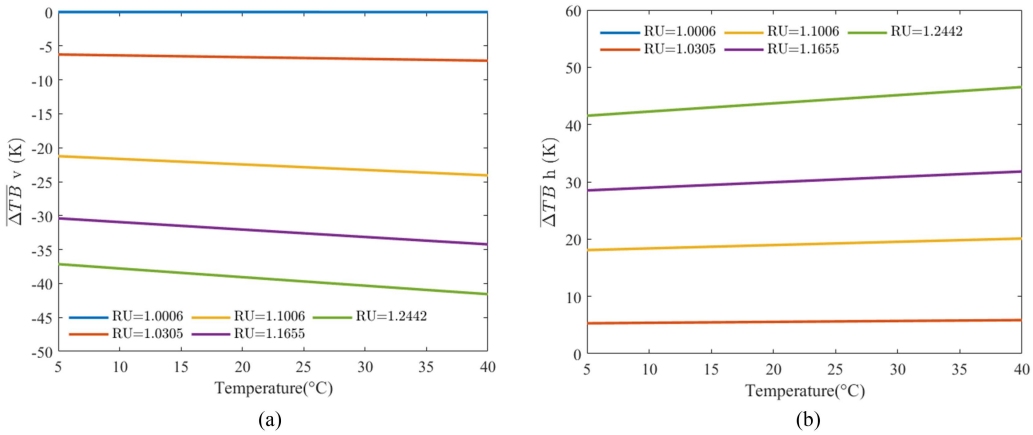

Fig. 10. Variations of $\overline{\Delta TB}$ with temperature in different topography regions. Different color represents different relief, the $\overline{\Delta TB}$ is the simulation result of microwave radiation when soil moisture is set to 0.25.

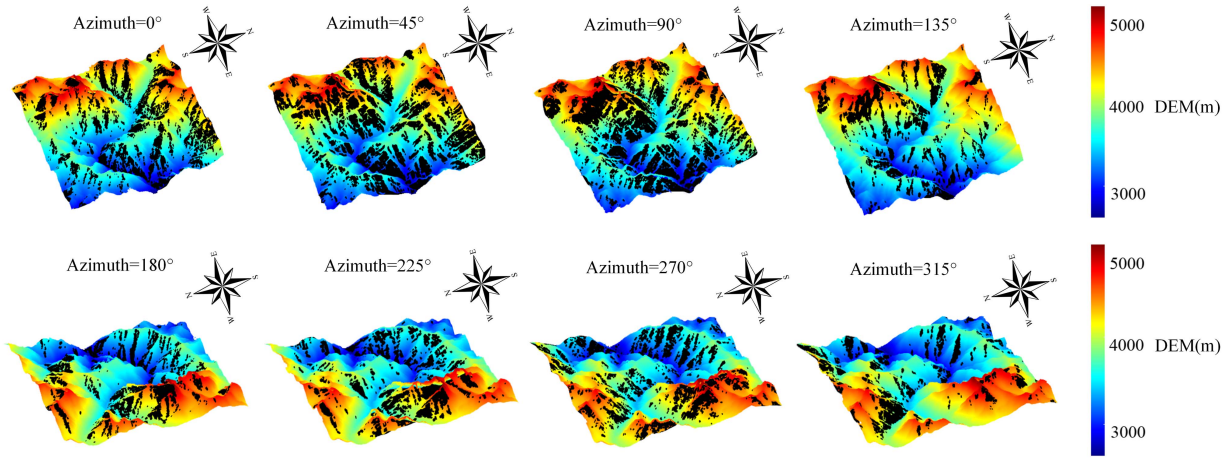

Fig. 11. Shading effect of the topography region for different observation orientations. The eight figures are shading effect at different observation directions in a pixel (0°–360°, step size 45°), the black area is the obstructed area. The upper and lower rows are displayed from two perspectives.

microwave radiation model is the aggregated brightness temperature of the surface brightness temperature of all non-black regions. For different topography regions, shading effect is also different.

The surface emissivity in Fresnel's formula is related to the $\cos(\theta)$ and $\cos^2(\chi)$. Therefore, we counted the ΔTB, $\cos(\theta)$ and $\cos^2(\chi)$ at different azimuths of pixels in different terrain surfaces [the $\cos(\theta)$ and $\cos^2(\chi)$ are the average of the observable surface units in the pixel], it is found that the relationship between ΔTB and $\cos(\theta)$ is linear. The trend of the fitted line varies with different topographic regions (see Fig. 12).

IV. Results

A. Terrain Correction Model

Based on the results in Section III, $\overline{\Delta TB}$ can be predicted according to RU and soil moisture. The $\overline{\Delta TB}$ is linearly related to RU.

According to Section III-C, α_{slope} and $\alpha_{\text{intercept}}$ are related to soil moisture. By calculating α_{slope} and $\alpha_{\text{intercept}}$ for different soil moisture (see Fig. 13), it can be found that α_{slope} and $\alpha_{\text{intercept}}$ change regularly with the change of soil moisture, and the fitted relationship between α_{slope} and $\alpha_{\text{intercept}}$, respectively, with soil moisture can be expressed accurately by quartic polynomial. The fitted results are given in Table II, these can be used to calculate the $\overline{\Delta TB}_{\text{model}}$ of terrain surface with different soil moisture.

The second part of the terrain correction model is to correct the effect of azimuth on ΔTB. According to Section III, the ΔTB is linearly related to $\cos(\theta)$, and the trend of the ΔTB with $\cos(\theta)$ varies with the RU of pixels. The fitted accuracy of ΔTB and $\cos(\theta)$ is shown in Fig. 14, the value of R^2 is above 0.9 for most pixels at *H* polarization and *V* polarization. As the RU increases, the R^2 decreases, this is because in addition to $\cos(\theta)$, the ΔTB is also affected by $\cos^2(\chi)$, and the effect of $\cos^2(\chi)$ is greater as RU increases. But for most terrain surface, the error caused by $\cos^2(\chi)$ is within the allowable range, and to simplify the calculation, this article only considers the impact of $\cos(\theta)$. Therefore, based on the slope of the fitting line of ΔTB and $\cos(\theta)$, $\cos(\theta)$, and $\overline{\Delta TB}_{\text{model}}$, the terrain correction model can be constructed to compute ΔTB_{model}.

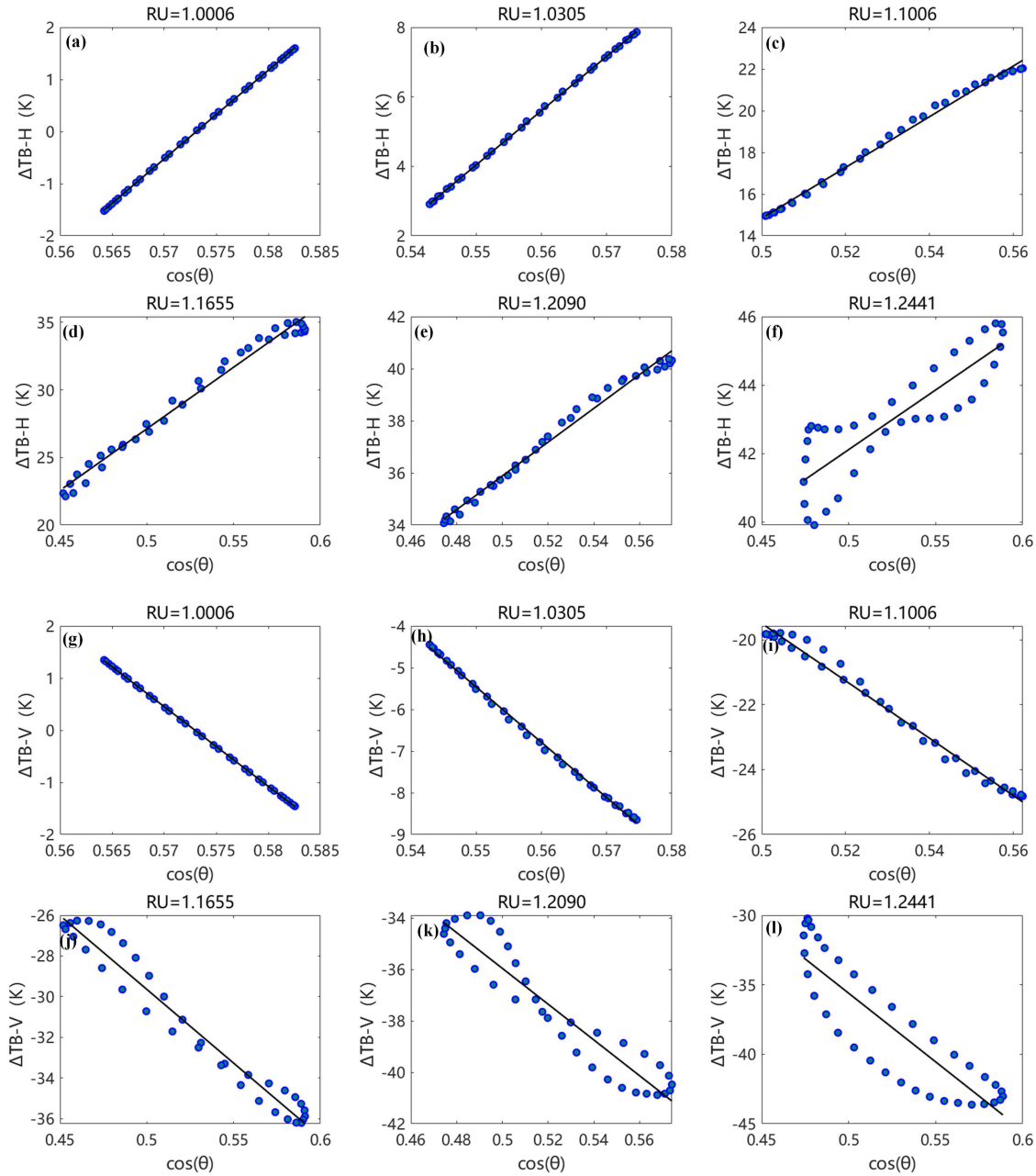

Fig. 12. Correlation between ΔTB and cos(θ) at different azimuths of pixels of different terrain surfaces.

TABLE II
FITTED COEFFICIENT AND STATISTICAL ERROR OF α_{SLOPE} AND $\alpha_{INTERCEPT}$ WITH SOIL MOISTURE

Polarization	Fitting function of α_{slope} and $\alpha_{intercept}$ with soil moisture (sm)	R^2	RMSE
H	$\alpha_{slope} = -6880sm^4 + 9653sm^3 - 5159sm^2 + 1225sm + 78.1$	0.9994	4.136
	$\alpha_{intercept} = 6838sm^4 - 9588sm^3 + 5119sm^2 - 1212sm - 79.6$	0.9994	4.130
V	$\alpha_{slope} = 5580sm^4 - 8143sm^3 + 4572sm^2 - 1117sm - 86.51$	0.9997	2.633
	$\alpha_{intercept} = -5507sm^4 + 8049sm^3 - 4532sm^2 + 1114sm + 84.49$	0.9997	2.577

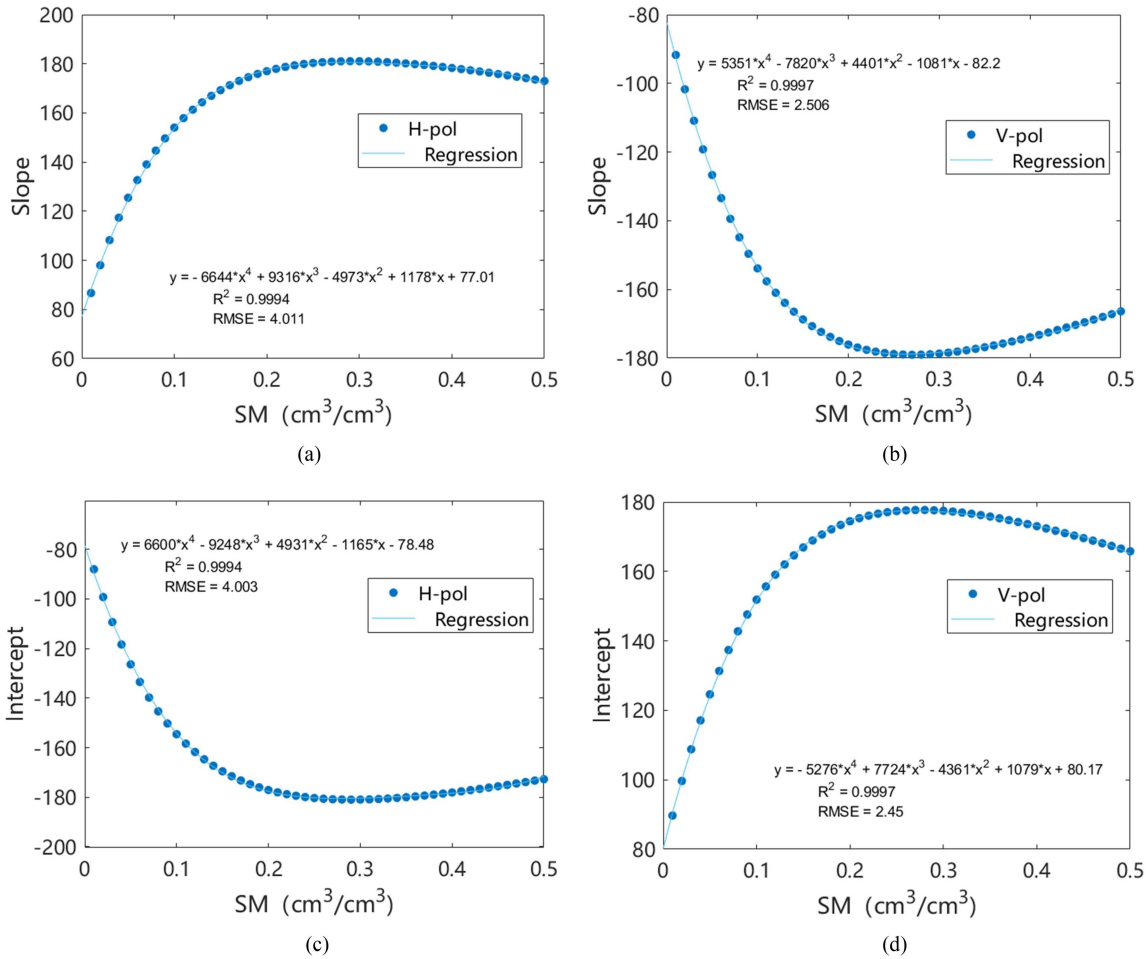

Fig. 13. Variation of the slope and intercept of the fitted curve of $\overline{\Delta TB}$ and RU with soil moisture. The blue dots represent the values of α slope and α intercept in equation (14) for different soil moisture.

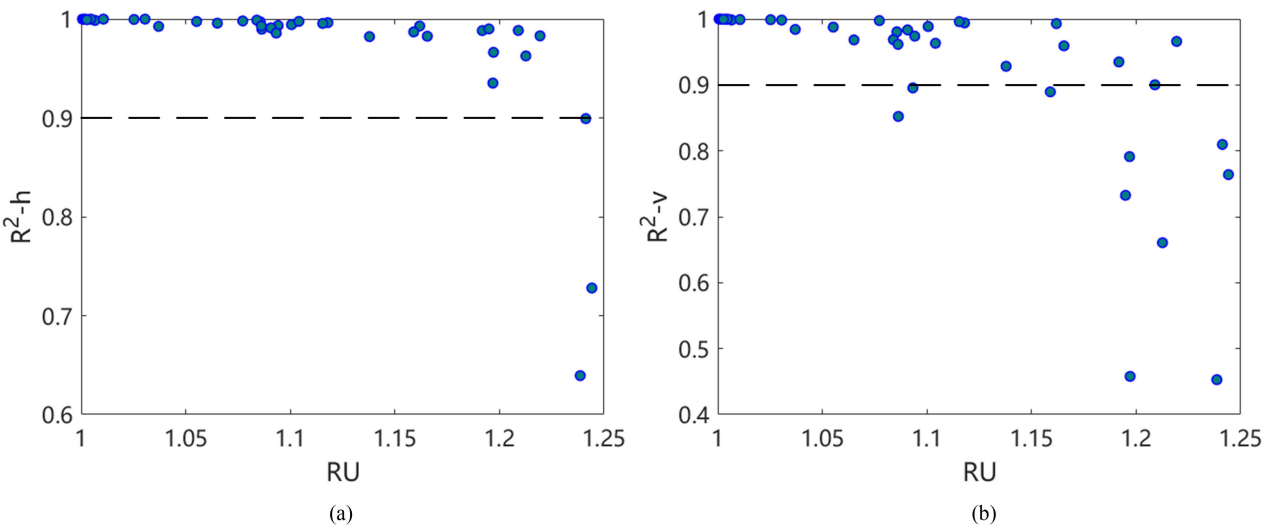

Fig. 14. Fitting accuracy of ΔTB and $\cos(\theta)$ for different topographic region.

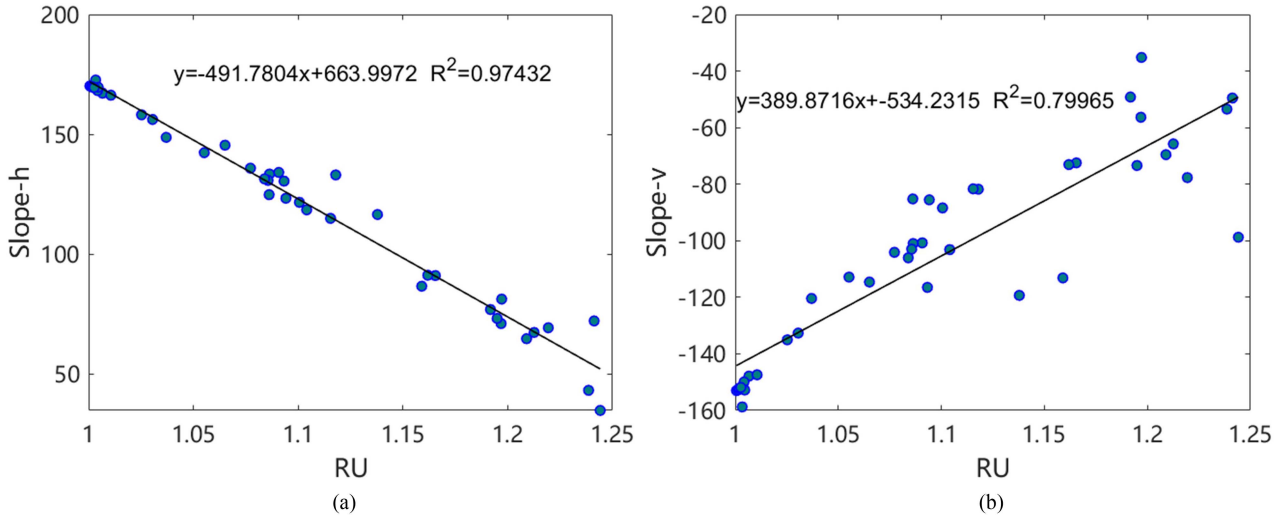

Fig. 15. Correlation between β_{slope} and RU for different topographic regions.

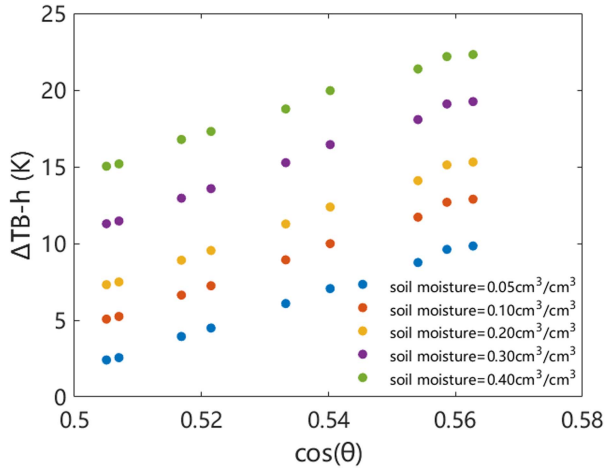

Fig. 16. Variation of ΔTB with $\cos(\theta)$ for different soil moisture (different colors represent ΔTB for different soil moisture inputs).

By calculating β_{slope} for topographic regions with different RUs, it can be discovered that the β_{slope} is linearly related to RU (see Fig. 15). In addition, ΔTB varies greatly at different soil moisture for the same pixel. Fig. 16 shows the variation of ΔTB with $\cos(\theta)$ for different soil moisture, the β_{slope} remains unchanged when the soil moisture is different. As a result, the effect of soil moisture should not be considered when correcting the effect of azimuth on ΔTB.

B. Model Validation

To validate the model in other terrain surfaces, simulations were also done over the region of the Hengduan Mountains and the Daxinganling Mountains. These two mountains regions were selected because the topography of the two mountains region is very different from that of the Qilian Mountains. The Hengduan Mountains are located in the southeastern part of the Tibetan Plateau, and consist of a series of north-south parallel mountains. The Daxinganling Mountains are located in Northeast China,

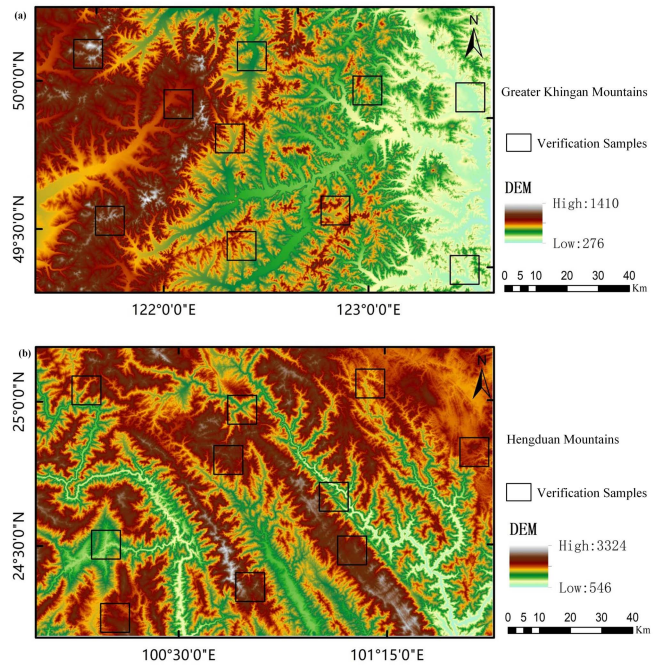

Fig. 17. Regions of the Hengduan mountains and the Daxing–Anling mountains.

the terrain is high in the west and low in the east. A total of ten separate regions of approximately 10 km × 10 km with different topography have been selected for the Validation in each mountain area. These regions are shown in Fig. 17 by the boxes with black boundaries. Statistically, these regions have different degrees of topographic relief, with RU values ranging from 1 to 1.2. The RU values of these regions are given in Table III. The DEMs of the regions have a resolution of 30 m and are obtained from the SRTM.

The proposed technique of topographic correction is verified by comparing the simulated brightness temperature differences of the microwave radiation model ($\Delta TB_{\text{simulated}}$) with the simulated values of the empirical model (ΔTB_{model}). Considering

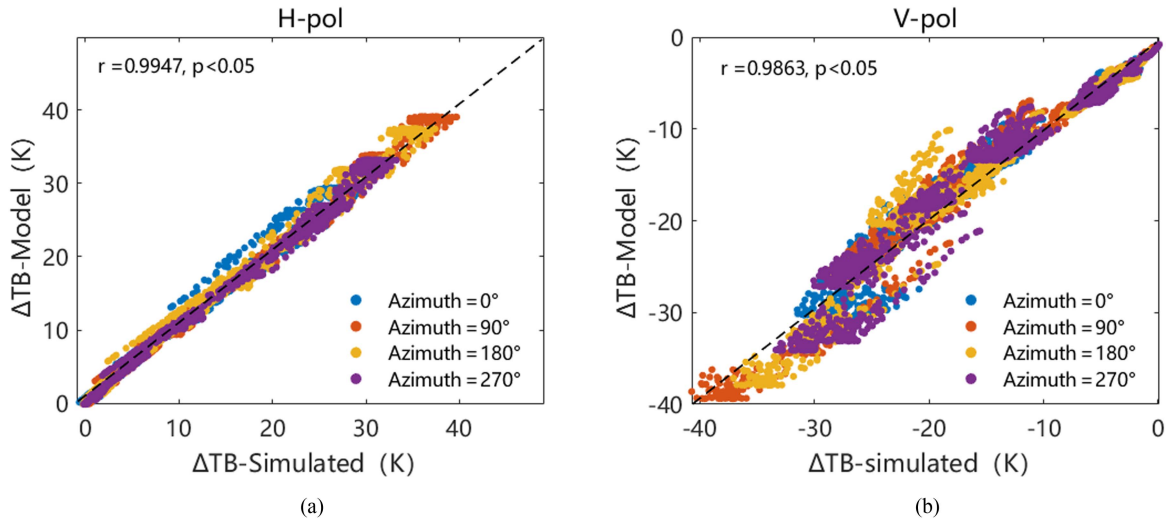

Fig. 18. Comparison of ΔTB simulated by the mountain microwave radiation model and empirical model for 20 regions of the Hengduan Mountains and the Daxinganling Mountains for horizontal (a) and vertical (b) polarization. The black dotted line is the 1:1 line.

TABLE III
RU VALUES OF 20 VALIDATION REGIONS FOR THE HENGDUAN MOUNTAINS AND THE DAXINGANLING MOUNTAINS

DEM	RU	DEM	RU
HD01	1.097044	DX01	1.026629
HD02	1.192112	DX02	1.015948
HD03	1.137151	DX03	1.032212
HD04	1.068327	DX04	1.025612
HD05	1.175631	DX05	1.028560
HD06	1.083220	DX06	1.009804
HD07	1.060742	DX07	1.027536
HD08	1.120442	DX08	1.021262
HD09	1.068955	DX09	1.033546
HD10	1.123440	DX10	1.009663

the influence of soil moisture and temperature, for each region, brightness temperatures at 100 different soil moisture and temperatures were simulated repeatedly, with the values randomly taken from a specific range (temperature of 5∼–40 °C; soil moisture for 0.01–0.50 cm^3/cm^3). The impact of topography was computed for each pixel at different soil moisture and temperature by the empirical model and using the microwave radiation model. The results are compared in Fig. 18(a) for horizontal polarization and Fig. 18(b) for vertical polarization. In this figure, the horizontal and vertical axes correspond to $\Delta TB_{\text{simulated}}$ and ΔTB_{model}, respectively.

The overall similarity between the results of two approaches is good in both polarizations, with *r* of 0.9947 in horizontal polarization and 0.9863 in vertical polarization. There is however a few bias between the two approaches. The bias, measured as the mean difference in ΔTB calculated by the two approaches, is between 0.1 K and 0.14 K for both polarizations. This bias may be inherited from the fitted error between $\overline{\Delta TB}$ and RU, and the fitted error between the slope of ΔTB and $\cos(\theta)$ with RU. In this figure, points of different colors represent brightness temperatures at different azimuth angles. Compared to vertical polarization, the accuracy of empirical model is greater in horizontal polarization, because the fitted accuracy of ΔTB and $\cos(\theta)$ is better in horizontal polarization.

V. DISCUSSIONS

Microwave radiation in undulating surface areas includes as follows.

1) Microwave radiation of each surface pixel that is observed by the radiometer after atmospheric attenuation.
2) The scattering of the surrounding radiation by the surface pixel observed by the radiometer after atmospheric attenuation. The ambient radiation includes the downward radiation of the atmosphere and the radiation of the mountains around the bin.
3) The upward radiation of the atmosphere itself. In the article, to highlight the impact of terrain itself, we chose to start with a simple surface scene. That is, the ground surface is assumed to be smooth, and the effects of vegetation, atmosphere and mountain radiation are not considered (see Section II).

In Section III-C, we have analyzed the influence of soil moisture on microwave radiation simulation in mountain areas. The results showed that the influence of soil moisture was quite significant. Therefore, when we simulated the brightness temperature in mountain areas, soil moisture was required as an input parameter of the model to improve the performance of our results. With the improved brightness temperature, the soil moisture could be better inverted. In our thoughts, we could first use soil moisture data of relatively low resolution as the input. Then, the corrected brightness temperature was used to invert soil moisture. Through multiple iterative optimizations, soil moisture of higher resolution and accuracy was obtained. We have not realized this method now, and it will be our task to verify this hypothesis in the future research.

VI. Conclusion

Topography can be significant for passive microwave remote sensing of soil moisture for mountainous surfaces. One problem with assessing topography's importance is that the DEMs cannot provide intuitive estimates of relief effects for pixel scale surfaces. To address this issue, RU is used instead of DEM to express the topographic relief of pixel scale surface, the microwave radiation model is used to simulate the topographic effects of topography regions with different RU. According to the evaluation of topographic effects, a new topographic correction method is established by regression analysis of topographic effects and RU. The conclusions are as follows.

RU calculated based on DEM as the relief of land surface has a linear relationship with $\overline{\Delta TB}$ for different topography regions, with R^2 above 0.9 for both polarizations. As the RU increases, the $\overline{\Delta TB}$ increases in horizontal polarization and decreases in vertical polarization.

Soil moisture greatly influences $\overline{\Delta TB}$, and the influence increases with increased RU. Different soil moisture can cause $\overline{\Delta TB}$ to vary by up to 21K. The fitted coefficients of $\overline{\Delta TB}$ and RU are related to soil moisture, the relationship between the fitted coefficients with soil moisture can be expressed by the quartic polynomial, with the value of R^2 above 0.99 for both polarizations.

Topographic effects are varied at different azimuths. The relationship between ΔTB and $\cos(\theta)$ is linear, and the trend of the fitted line varies with different topographic regions. The slope of the fitted line is also linearly related to RU, with the value of R^2 above 0.9 for horizontal polarization and above 0.8 for vertical polarization.

The terrain correction model is proposed based on the regression analysis between ΔTB, Topographic effects, and RU. According to the model validation results, the model applies to different mountainous regions and can accurately correct the microwave radiation error caused by arbitrary topography and observation orientation. These results provide a new approach and an effective method to eliminate the influence of topography in microwave remote sensing, which is of great significance in improving the inversion accuracy of surface soil moisture in mountainous regions. In the future, we need to further study the topographic effects of rough and vegetation-covered surfaces in mountainous regions, and supplement and improve the terrain correction model.

References

[1] K. Jonas, B. André, A. J. Dietz, and K. Claudia, "Towards forecasting future snow cover dynamics in the European Alps—The potential of long optical remote-sensing time series," *Remote Sens.*, vol. 14, no. 18, 2022, Art. no. 4461.

[2] Y. Shengtian et al., "Remote sensing hydrological indication: Responses of hydrological processes to vegetation cover change in mid-latitude mountainous regions," *Sci. Total Environ.*, vol. 851, no. P1, 2022, Art. no. 158170.

[3] A. Li et al., "Remote sensing inversion modeling and spatiotemporal characterization of typical ecological parameters in mountainous areas," *Adv. Earth Sci.*, vol. 33, no. 02, pp. 141–151, 2018.

[4] W. Zhao, P. Huang, and A. Li, "Research status of remote sensing estimation of surface evapotranspiration in mountainous areas," *J. Mountain Sci.*, vol. 35, no. 6, pp. 908–918, 2017.

[5] I. D. Moore, "Topographic effects on the distribution of surface soil water and the location of ephemeral gullies," *Trans. Amer. Soc. Agricultural Engineers*, vol. 31, no. 4, pp. 1098–1107, 1988.

[6] A. N. Flores, V. Y. Ivanov, D. Entekhabi, and R. L. Bras, "Impact of hillslope-scale organization of topography, soil moisture, soil temperature, and vegetation on modeling surface microwave radiation emission," *IEEE Trans. Geosci. Remote Sens.*, vol. 47, no. 8, pp. 2557–2571, Aug. 2009.

[7] T. Pellarin et al., "Three years of L-band brightness temperature measurements in a mountainous area: Topography, vegetation and snowmelt issues," *Remote Sens. Environ.*, vol. 180, pp. 85–98, 2016.

[8] Q. Xie, L. Ja, Q. Chen, Y. Yin, and M. Menenti, "Evaluation of soil moisture products by microwave remote sensing in the farming-pastoral ecotone of the Lightning River Basin," *Remote Sens.*, vol. 25, no. 4, pp. 974–989, 2021.

[9] J. Liu et al., "Uncertainty analysis of eleven multisource soil moisture products in the third pole environment based on the three-corned hat method," *Remote Sens. Environ.*, vol. 255, 2021, Art. no. 112225.

[10] L. Li, D. Wu, T. Wang, and Y. Wang, "Effect of topography on spatiotemporal patterns of soil moisture in a mountainous region of Northwest China," *Geoderma Regional*, vol. 28, 2022, Art. no. e456.

[11] X. Li, L. Zhang, L. Jiang, S. Zhao, and T. Zhao, "Simulation and measurement of relief effects on passive microwave radiation," in *Proc. IEEE Int. Geosci. Remote Sens. Symp.*, 2010, pp. 3015–3018.

[12] C. Maetzler and A. Standley, "Technical note; relief effects for passive microwave remote sensing," *Int. J. Remote Sens.*, vol. 21, no. 12, pp. 2403–2412, 2000.

[13] Y. H. Kerr, F. Secherre, J. Lastenet, and J.-P. Wigneron, "SMOS: Analysis of perturbing effects over land surfaces," in *Proc. IEEE Int. Geosci. Remote Sens. Symp.*, 2003, pp. 908–910.

[14] A. Mialon, L. Coret, Y. H. Kerr, F. Secherre, and J.-P. Wigneron, "Flagging the topographic impact on the SMOS signal," *IEEE Trans. Geosci. Remote Sens.*, vol. 46, no. 3, pp. 689–694, Mar. 2008.

[15] M. Talone, A. Camps, A. Monerris, M. Vall-llossera, P. Ferrazzoli, and M. Piles, "Surface topography and mixed-pixel effects on the simulated L-band brightness temperatures," *IEEE Trans. Geosci. Remote Sens.*, vol. 45, no. 7, pp. 1996–2003, Jul. 2007.

[16] L. Pulvirenti, N. Pierdicca, and F. S. Marzano, "Prediction of the error induced by topography in satellite microwave radiometric observations," *IEEE Trans. Geosci. Remote Sens.*, vol. 49, no. 9, pp. 3180–3188, Sep. 2011.

[17] L. Pulvirenti, N. Pierdicca, and F. S. Marzano, "Topographic effects on the surface emissivity of a mountainous area observed by a spaceborne microwave radiometer," *Sensors*, vol. 8, no. 3, pp. 1459–1474, 2008.

[18] C. Utku and D. M. Le Vine, "A model for prediction of the impact of topography on microwave emission," *IEEE Trans. Geosci. Remote Sens.*, vol. 49, no. 1, pp. 395–405, Jan. 2011.

[19] Y. Guo, J. Shi, J. Du, and X. Fu, "Evaluation of terrain effect on microwave radiometer measurement and its correction," *Int. J. Remote Sens.*, vol. 32, no. 24, pp. 8899–8913, 2011.

[20] X. Li, L. Zhang, L. Jiang, and S. Zhao, "Effects of mountain terrain on microwave radiation characteristics and soil moisture retrieval-taking the Qinghai-Tibet Plateau as an example," *J. Remote Sens.*, vol. 16, no. 4, pp. 850–867, 2012.

[21] A. Monerris et al., "Topography effects on the L-band emissivity of soils: TuRTLE 2006 field experiment," in *Proc. IEEE Int. Geosci. Remote Sens. Symp.*, 2007, pp. 2244–2247.

[22] N. Pierdicca, L. Pulvirenti, and F. S. Marzano, "A simulation study to quantify the relief effects on the observations performed by microwave radiometers," in *Proc. IEEE Int. Geosci. Remote Sens. Symp.*, 2008, pp. II–684–II–686.

[23] A. Camps et al., "Sensitivity of GNSS-R spaceborne observations to soil moisture and vegetation," *IEEE J. Sel. Topics Appl. Earth Observ. Remote Sens.*, vol. 9, no. 10, pp. 4730–4742, Oct. 2016.

[24] M. J. Sandells, I. J. Davenport, and R. J. Gurney, "Passive L-band microwave soil moisture retrieval error arising from topography in otherwise uniform scenes," *Adv. Water Resour.*, vol. 31, no. 11, pp. 1433–1443, 2008.

[25] G. Kirchhoff, "I. On the relation between the radiating and absorbing powers of different bodies for light and heat," *London, Edinburgh Dublin Philos. Mag. J. Sci.*, vol. 20, no. 130, pp. 1–21, 1860.

[26] M. C. Dobson, F. T. Ulaby, M. T. Hallikainen, and M. A. El-rayes, "Microwave dielectric behavior of wet soil-Part II: Dielectric mixing models," *IEEE Trans. Geosci. Remote Sens.*, vol. GE-23, no. 1, pp. 35–46, Jan. 1985.

[27] R. D. Hobson, *FORTRAN IV Programs to Determine Surface Roughness in Topography for the CDC 3400 Computer*. Lawrence, KS, USA: Univ. Kansas, 1967.
[28] H. Lu, X. Liu, and G. Tang, "Multi-factor comprehensive evaluation method of terrain complexity," *J. Mountain Sci.*, vol. 30, pp. 616–621, 2012.
[29] F. Jiang, C. Zhu, and X. Li, "DEM topographic factor and its application," in *Proc. 9th Annu. Conf. China Geographic Inf. Syst. Assoc.*, 2005, pp. 699–704.
[30] L. D. Landau, E. M. Lifshitz, J. B. Sykes, J. S. Bell, and E. H. Dill, "Electrodynamics of continuous media," *Phys. Today*, vol. 14, no. 10, pp. 48–50, 1961.

Shaojie Zhao (Member, IEEE) received the B.S. degree in geography and the Ph.D. degree in cartography and geography information system from Beijing Normal University, Beijing, China, in 2006 and 2011, respectively.

He is currently a Laboratory Experimentalist with the Faculty of Geographical Science, Beijing Normal University. His interests are passive microwave remote sensing of soil moisture and frozen soil.

Ting Liu received the B.S. degree in food science and engineering from the Yibin University, Yibin, China, in 2019, and the M.S. degree in cartography and geography information system from the Xinjiang University, Urumqi, China, in 2022.

In 2023, she was with the Land Satellite Remote Sensing Application Center, Beijing, China. Her research interest focuses on passive microwave remote sensing of soil moisture.

Linna Chai (Member, IEEE) received the B.E. degree in computer science and technology fromthe Wuhan University of Technology, Wuhan, China, in 2002, and the Ph.D. degree in geography from Beijing Normal University, Beijing, China, in 2010.

She is currently an Associate Professor with the Facultyof Geographical Science, Beijing Normal University. Her research interests include microwave remotesensing, and modeling and retrieving of vegetationand soil properties.

Peng Wang received the B.S. degree in surveying and mapping engineering of Shijiazhuang Tiedao University, Shijiazhuang, China, in 2019. He is currently working toward the M.Sc. degree in cartography and geography information system with Jilin university, Jilin, China.

His research interest focuses on passive microwave retrieval of surface soil moisture in mountainous areas.

Diyan Chen received the B.S. degree in geographic information systems from the Southwest University, Chongqing, China, in 2021. She is currently working toward the Postgraduate degree in quantitative remote sensing with the Beijing Normal University, Beijing, China.

Her research involves using satellite remote sensing, models, and fieldwork to retrieve and understand how corn's moisture content varies during the maize growth period.

Tao Zhang received the B.S. degree in geographic information system of Shandong Jianzhu University, Jinan, China, in 2008, and the M.S. and Ph.D. degrees in cartography and geography information system from the Beijing Normal University, Beijing, China, in 2011 and 2014, respectively.

In 2014, he was with the Land Satellite Remote Sensing Application Center, Beijing, China, where he is currently a Senior Engineer. His research interest mainly focuses on the integrated application of satellite remote sensing in land use, urban development and environmental monitoring.